

# CO<sub>2</sub>-Induced Microstructure Transition of Surfactant in Aqueous Solution: Insight from Molecular Dynamics Simulation

Shengchi Zhuo,<sup>†</sup> Yongmin Huang,<sup>†</sup> Changjun Peng,<sup>†</sup> Honglai Liu,<sup>\*,†</sup> Ying Hu,<sup>†</sup> and Jianwen Jiang<sup>‡</sup>

Key Laboratory for Advanced Material and Department of Chemistry, East China University of Science and Technology, Shanghai 200237, China, and Department of Chemical and Biomolecular Engineering, National University of Singapore, 117576, Singapore

Received: October 27, 2009; Revised Manuscript Received: January 18, 2010

A molecular dynamics simulation study is reported to investigate a CO<sub>2</sub>-induced microstructure transition of surfactant AOT4 in aqueous solution. The lamellar bilayer changes into a spherical micelle induced by CO<sub>2</sub> at ambient temperature, while a thermotropic aggregate occurs in the absence of CO<sub>2</sub> above 140 °C. In the lamellar bilayer, AOT4 shows a bimodal density distribution. The bilayer thickness and the average area per AOT4 are estimated to be 19.2 Å and 83.3 Å<sup>2</sup>. The AOT4 bilayer possesses a sandwich structure and consists of a hydrophobic region in the center and a hydrated layer on both sides. Upon CO<sub>2</sub> dissolving, the lamellar bilayer is swollen and becomes loose and unstable. CO<sub>2</sub> molecules in the lamellar bilayer are initially near the ester groups of AOT4 and then accumulate in the center of the hydrophobic region. With increasing amounts of CO<sub>2</sub>, the AOT4 bilayer expands gradually and the density distribution of each leaflet becomes broader. Driven by surface tension, the lamellar bilayer tends to reduce the surface area. The lamellar bilayer changes into a 3D cubic network in a small simulation box, attributed to the influence of neighboring images. In a sufficiently large box, the lamellar bilayer transforms into spherical micelles. CO<sub>2</sub>-active surfactants such as fluorinated surfactants and oxygenated AOT analogues are proposed to substitute CO<sub>2</sub>-inactive AOT and may reduce the critical pressure in microstructure transition.

## 1. Introduction

Commonly used in soaps and detergents,<sup>1</sup> emulsification,<sup>2</sup> and enhancing oil recovery,<sup>3</sup> surfactants show remarkable surface/interface activity. Because of the amphiphilic nature with both hydrophilic and hydrophobic moieties, surfactants in aqueous solution can assemble to form a variety of ordered microstructures beyond the critical micelle concentration (cmc), such as spherical and cylindrical micelles, lamellar bilayers, vesicles, and liquid crystals. The microstructure of surfactant aggregations plays a central role in tuning the properties and performances of surfactant solutions. Most of the practical applications of surfactants are based on their specified microstructures, for example, in drug delivery,<sup>4</sup> model membrane,<sup>5</sup> and templates for synthesis of nanomaterials.<sup>6–11</sup> The influences of surfactant, cosurfactant, and their compositions were recently examined on the size, morphology and ratio of one-dimensional nanomaterials.<sup>11</sup> Surfactants with special microstructures were used as templates for the synthesis of ordered mesoporous materials.<sup>12,13</sup>

To fabricate a specific template, it is important to govern the microstructures of surfactant aggregations. They can be triggered by additives, dilution, chemical reaction, and changing temperature/pressure. In addition, they could be induced by applying external fields such as shear, electric, or magnetic field.<sup>14</sup> Through small angle neutron scattering, Imai et al. studied the transition between lamellar and gyroidal morphologies induced by shearing.<sup>15</sup> The shear-induced transition of lamellar phase into vesicle phase was also studied by Escalante et al.<sup>16</sup> Richtering et al. reviewed the rheology and shear-induced

structures in surfactant solutions.<sup>17</sup> Dan and co-workers investigated the effect of mixing on microstructure transition in aqueous solution of surfactant Triton X-100 and diblock polymer PBD-PEO.<sup>18</sup> Nakamura et al. estimated the influence of surfactant content on morphology and observed a transition from lamellar phase to microemulsion in water/sucrose monododecanoate/hexanol/decane by decreasing surfactant content.<sup>19</sup> Macdonald et al. reported a thermotropic phase transition in polyelectrolyte–surfactant system of PACA/CTAB/HDPC, in which the hexagonal liquid crystal phase (H<sub>I</sub>) was found to change into lamellar bilayer (L<sub>α</sub>) by decreasing temperature.<sup>20</sup> Wang studied the influence of pH on the microstructures of surfactant bis(amidoethyl-carbamoylethyl) octadecylamine in aqueous solution. The surfactant was observed to form micelles, vesicle, and lamellar structure at pH = 2.0, 6.8, and 12.0, respectively.<sup>21</sup> Gradielski reviewed the kinetics of microstructure transition in surfactant systems.<sup>14</sup>

Recently, Zhang et al. reported a reversible microstructure transition between lamellar (L<sub>α</sub>) and micellar (L<sub>1</sub>) phases for surfactant Aerosol OT (AOT) induced by compressed CO<sub>2</sub>.<sup>22</sup> With increasing CO<sub>2</sub> pressure, the lamellar bilayer of AOT was swollen due to the dissolved CO<sub>2</sub> in the hydrophobic layer. The lamellar phase changed to micellar at CO<sub>2</sub> pressure higher than a critical pressure  $p_T$ . The microstructure transition was reversed by reducing CO<sub>2</sub> pressure. The phase transition from L<sub>α</sub> to L<sub>1</sub> induced by CO<sub>2</sub> could be achieved at ambient temperature, while a similar phase transition occurred above 140 °C without CO<sub>2</sub>. The postprocessing of this method is much easier than conventional methods, in which additives (e.g., cosurfactants, salts) have to be removed. Though the microstructure transition induced by CO<sub>2</sub> is superior to conventional methods in many aspects, the mechanism of this process is not well understood.

\* Corresponding author. E-mail: hlliu@ecust.edu.cn (H. Liu).

<sup>†</sup> East China University of Science and Technology.

<sup>‡</sup> National University of Singapore.

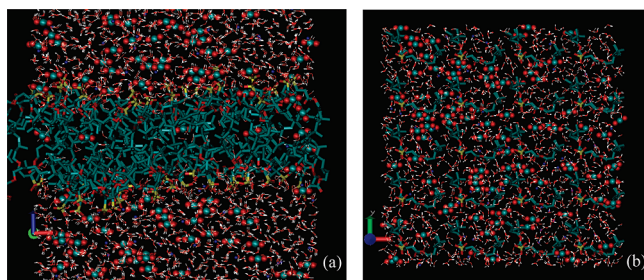


**Figure 1.** Initial structures in simulations (a) with a preformed lamellar bilayer and (b) with homogeneously distributed surfactants. Surfactant is in the bond model, water in line, counterion in the ball model, and CO<sub>2</sub> is highlighted by CPK model. Color code: O, red; H, white; Na<sup>+</sup>, blue; C, cyan; S, yellow.

In this work, molecular dynamics simulations are carried out to investigate the fundamental mechanism of CO<sub>2</sub>-induced microstructure transition at the atomistic level. Despite a large number of simulation studies reported for surfactant systems,<sup>23–26</sup> to the best of our knowledge, this is the first simulation study on the microstructure transition of surfactant induced by CO<sub>2</sub>. Following this section, the model and methodology used are described in section 2. In section 3, the density profiles of surfactant are characterized in the absence and presence of CO<sub>2</sub>. The process of CO<sub>2</sub> entering in the lamellar bilayer is examined by the time evolution of the density profile. The distribution of CO<sub>2</sub> inside the lamellar bilayer is also identified. The solvation of CO<sub>2</sub> and expansion of the lamellar bilayer are estimated and compared at various amounts of CO<sub>2</sub>. The speculated mechanism in microstructure transition induced by CO<sub>2</sub> is discussed. Thereafter, several CO<sub>2</sub>-active surfactants are suggested to substitute CO<sub>2</sub>-inactive AOT to reduce the critical pressure in microstructure transition. Finally, the conclusion remarks are summarized in section 4.

## 2. Model and Methodology

There are a series of AOT surfactants, which are named AOT1 to AOT7. They possess identical headgroups but different hydrocarbon tails.<sup>27</sup> In this work, AOT4 (sodium bis-3,5,5,-methyl-1-hexyl sulfosuccinate) was considered. Molecular dynamics simulations were performed in two different strategies. In the first case, 60 AOT4 surfactants were added in a cubic simulation box with length of 5 nm. Subsequently, the box was filled with water molecules and an appropriate number of Na<sup>+</sup> counterions were added to maintain system electroneutrality. MD simulation was carried out for 10 ns to form a lamellar bilayer. Thereafter, certain numbers of CO<sub>2</sub> molecules were added randomly in the system as shown in Figure 1a, followed by 10 ns simulation at 290 K. This process is analogous to the experimental work by Zhang et al.<sup>22</sup> However, due to the stability of lamellar bilayer, it was difficult for the lamellar bilayer to switch to other microstructures within the feasible simulation time. As a consequence, another initial structure was used for simulation. In this case, 60 AOT4 surfactants were placed homogeneously in the simulation box and a certain number of CO<sub>2</sub> molecules were added randomly in the box, as shown in Figure 1b. Then, MD simulation was performed for 10 ns to achieve the most stable microstructure. According to thermodynamic principles, two multicomponent systems with the same composition should reach a unique stable phase at the same conditions. Hence, the two cases mentioned above were expected to achieve the same final state. It was indeed observed in our simulations that both of these two strategies yielded similar structures, which consists of a lamellar bilayer.

AOT4 was mimicked by the united-atom model as illustrated in Figure S1 in the Supporting Information. The FFG53a6 united-atom force field<sup>28</sup> was used to model AOT4, in which each CH<sub>n</sub> group was regarded as a single interaction site. The pairwise additive interactions have two contributions, one is bonded and the other nonbonded. While the bonded interactions include stretching, bending, and proper and improper torsional potentials, the nonbonded interactions include Lennard-Jones (LJ 12–6) and Coulombic potentials. To evaluate the atomic partial charges of AOT4, the nonlocal density functional theory (DFT) was employed with the Becke exchange functional (B88)<sup>29</sup> in conjunction with the Lee–Yang–Parr correlation functional (LYP).<sup>30</sup> The DNP (double numerical plus polarization) basis set was adopted. In addition, the semicore pseudopotential was used allowing only the softer valence electron wave functions to be explicitly treated, which is usually the portion that controls the chemistry and can significantly reduce computational cost. After the DFT calculation, the Hirshfeld popular analysis<sup>31</sup> was used to estimate the partial charges. For united atoms of CH<sub>n</sub>, the partial charges were obtained by the summation of the corresponding atomic charges. The overall partial charges of AOT4 are listed in Supporting Information Table S1. The net charge of AOT4 is  $-e$  ( $e = 1.6022 \times 10^{-19}$  is the elementary charge).

*Gromacs v 3.3.1* simulation package was employed to perform our simulations. The Lennard-Jones interactions were calculated with a spherical cutoff distance of 1.4 nm. The particle-mesh-Ewald (PME) method was applied to calculate the Coulombic interactions, with a grid spacing of 0.12 nm and a fourth-order interpolation. The bond lengths with dangling hydrogen atoms in AOT4 were constrained using the LINCS algorithm. The water molecule was represented by the simple point charge/extended (SPC/E) model with and the geometry constrained by the SETTLE algorithm. The temperature was controlled by Berendsen thermostat with a relaxation time of 0.1 ps. The periodic boundary conditions were considered in three dimensions. Energy minimization was carried out with the steepest descent method. Thereafter, initial velocities were assigned to the system according to the Maxwell–Boltzmann distribution. Equilibrium simulation was performed in canonical ensemble (NVT) for 5 ns, followed by production simulation for another 5 ns. The integration time step was 2 fs, and the neighbor list and long-range forces were updated every 10 steps (0.02 ps). The atomic coordinates and velocities were saved every 500 steps (1 ps) for analysis.

## 3. Results and Discussion

Several systems with various amounts of AOT4 surfactants were simulated in the absence of CO<sub>2</sub>, and the system with 60 AOT4 was found to form a stable lamellar bilayer at 290 K. In our simulation, the thickness of the bilayer (without dissolved CO<sub>2</sub>) was found to be 19.2 Å, which is consistent with the thickness of the bilayer formed by AOT1 (19.5 Å).<sup>32</sup> It should be noted that bilayers formed by AOT1 and AOT4 are comparable because both of them possess a hydrocarbon tail with six carbons in the backbone. However, the average area per headgroup in our simulation is 83.3 Å<sup>2</sup>, which is greater than the experimental area (67 Å<sup>2</sup>), but close to the area in the air/water interface at cmc (86 Å<sup>2</sup>).<sup>32</sup> The simulated area is also greater than the value at cmc ( $70 \pm 2$  Å<sup>2</sup>) experimentally reported by Nave et al.<sup>33</sup> The difference between simulation and experimental results may be attributed to the inaccuracy of the force field parameters used. Figure 2a shows the density distributions along the normal direction of the bilayer in system

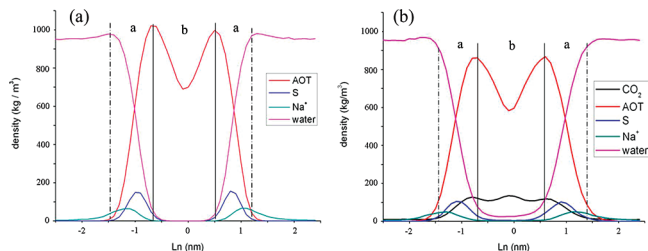


**Figure 2.** Density distributions along the normal direction of the lamellar bilayer in systems with 60 AOT4 surfactants and (a) 0 CO<sub>2</sub> and (b) 100 CO<sub>2</sub>. The x-axis stands for the length of simulation box in the normal direction of the lamellar bilayer.

with 60 AOT4 surfactants. The snapshot of the system is shown in Figure 3a. AOT4 shows a bimodal density distribution, which is in accord with the microstructure of the lamellar bilayer. Two density peaks are observed approximately at 2 and 3 nm, respectively. A trough is located between them due to the loose packing of hydrophobic tails. In this hydrophobic region of the lamellar bilayer, the density of water is nearly zero. The headgroups (S atom) of AOT4 distribute primarily in region a, which is the hydrophilic region of the lamellar bilayer. The headgroups are hydrated by water and reduce the interfacial tension between water and the hydrophobic layer of the bilayer. The Na<sup>+</sup> counterions are mainly distributed around headgroups due to the Coulombic interactions. Figure 2b shows the density distributions in the system with 60 AOT4 and 100 CO<sub>2</sub>. Compared to Figure 2a, the peaks of AOT4 are lower and the hydrophobic core expands slightly. The distributions of surfactants and counterions become broader. Most CO<sub>2</sub> molecules are dissolved in the lamellar bilayer and form three indistinct peaks. Two of them are located around the edge of the hydrophobic core and the third is in the center of the hydrophobic region.

With a strong quadrupole, CO<sub>2</sub> is expected to dissolve around the headgroups due to the electrostatic interaction. As shown in Figure 4, however, the density peaks of CO<sub>2</sub> are located at the same region with the ester groups of AOT4 rather than the headgroups. This might be due to the hydrophobicity of CO<sub>2</sub> which restricts its distribution in the hydrated layer. In addition, the polar ester groups have preferential affinity for CO<sub>2</sub>. Figure 5 shows the density distribution of CO<sub>2</sub> at different simulation durations. In the early stage, CO<sub>2</sub> distributes randomly in the box, mainly in the water phase. With the progress of simulation, CO<sub>2</sub> gradually aggregates around ester groups and at the center of hydrophobic region.

As mentioned above, CO<sub>2</sub> prefers to be localized around the ester groups. Hence, CO<sub>2</sub> forms two density peaks at a low concentration as shown in Figure 6a. These two peaks are expected to be symmetric because of the equivalence of the bilayer leaflets. A number of CO<sub>2</sub> molecules also distribute homogeneously in the layer of hydrocarbon tails, as shown intuitively in Figure 3b. With increasing amounts of CO<sub>2</sub>, more CO<sub>2</sub> molecules locate in the hydrophobic region, and then, the third peak of CO<sub>2</sub> appears in the center of the hydrophobic region. With more CO<sub>2</sub> in the system, the amount of CO<sub>2</sub> in the center of the hydrophobic core grows more predominantly than those in the ester group region. In a system with 200 CO<sub>2</sub> molecules, the density peak in the center of the hydrophobic region is much higher than the other two peaks. As shown in Figure 6b, the lamellar bilayer is swollen by dissolved CO<sub>2</sub>. The density peaks of AOT4 decrease and the lamellar bilayer expands in the normal direction as CO<sub>2</sub> molecules accumulate at the hydrophobic core. This is consistent with the X-ray diffraction results obtained by Zhang et al.<sup>22</sup>

The lamellar bilayer becomes loose and unstable swollen by CO<sub>2</sub>. To reduce the total energy of the system, the surface area of lamellar bilayer tends to shrink, driven by surface tension and relative thermodynamic factors. It is well-known that a sphere possesses the greatest volume than other geometric bodies with the same surface area. As a result, the lamellar bilayer is not able to keep its microstructure and subsequently changes into a spherical micelle when the amount of CO<sub>2</sub> exceeds a specific critical value. In the experiment of Zhang and co-workers,<sup>22</sup> the lamellar bilayer was observed to transform into a spherical micelle at CO<sub>2</sub> pressure about 4.85 MPa. In our simulation with 300 CO<sub>2</sub> molecules in the system, we found the lamellar bilayer changed into a 3D cubic network as shown in Figure 7a. The possible reason for this might be that the simulation box was not sufficiently large, and the transition from the lamellar bilayer to the spherical micelle was influenced by the neighboring images. As a consequence, the spherical micelles connected with each other to form the 3D cubic network. To avoid the influence of neighboring images, the simulation box was increased to 8 × 8 × 8 nm<sup>3</sup>. The numbers of AOT4, counterions, and CO<sub>2</sub> were increased proportionally. With the larger simulation box, the spherical micelles induced by CO<sub>2</sub> were observed as shown in Figure 7b.

The microscopic information from simulation complements experimental observation and could give insight into mechanism in the microstructure transition of surfactant induced by CO<sub>2</sub>. On the basis of the information mentioned above, the process of microstructure transition of the lamellar bilayer is speculated as four steps: (1) CO<sub>2</sub> dissolves in aqueous solution. (2) CO<sub>2</sub> enters the lamellar bilayer near the ester groups. The lamellar bilayer packs loosely as swollen by CO<sub>2</sub>. (3) Condensed CO<sub>2</sub> layer is formed in the center of hydrophobic region of the lamellar bilayer, which results in the expansion of the lamellar bilayer. (4) The lamellar bilayer collapses and changes into the spherical micelle due to the free energy of system.

At the surfactant concentration discussed in this work, the lamellar bilayer is more stable than the spherical micelle. Microstructure transition is triggered by CO<sub>2</sub> because the addition of CO<sub>2</sub> changes the Gibbs free energy of the system. The solubility of gas in water is a monotonic increasing function of gas pressure  $p_{CO_2} \propto [CO_2]_{water}$ .

For example, Henry's Law is validated for the solubility of most gases at low pressures. For surfactant solution (greater than cmc), dissolved CO<sub>2</sub> distributes in both water and micelle phases, which is a dynamic equilibrium.



The equilibrium constant  $K^\ominus$ , which is also considered the distribution factor,<sup>34</sup> can be expressed as

$$K^\ominus = \frac{[CO_2]_{micelle}}{[CO_2]_{water}} \quad (2)$$

As the solubility of CO<sub>2</sub> in water is proportional to the pressure of CO<sub>2</sub>, combined with eq 2, we can obtain the following expression:

$$p_{tran,CO_2} \propto \frac{[CO_2]_{micelle}^c}{K^\ominus} \quad (3)$$

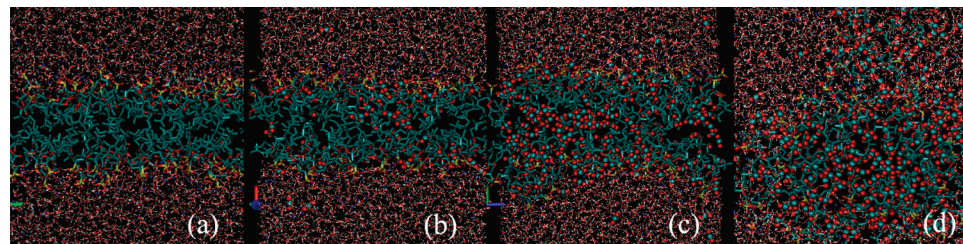


**Figure 3.** Simulation snapshots in systems with 60 AOT4 surfactants and (a) 0 CO<sub>2</sub>, (b) 60 CO<sub>2</sub>, (c) 200 CO<sub>2</sub>, and (d) 300 CO<sub>2</sub>. Display model and color code are the same as Figure 1.

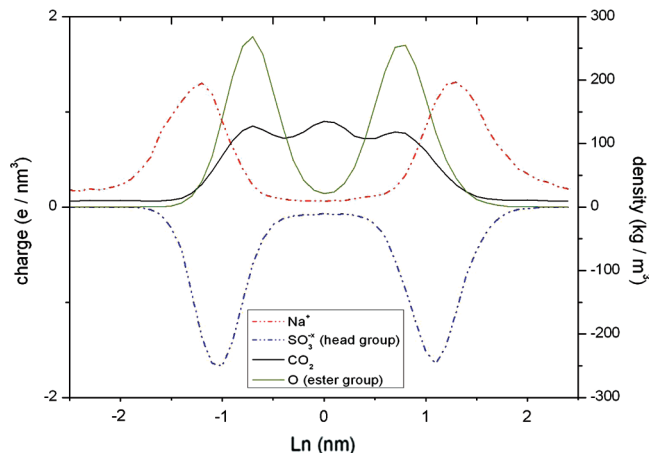


**Figure 4.** Density distributions of CO<sub>2</sub> and O atom of ester group in AOT4 and charge distributions of the headgroup of AOT4 and counterion Na<sup>+</sup>. Solid lines represent the density distributions, while dashed lines represent the charge distributions.

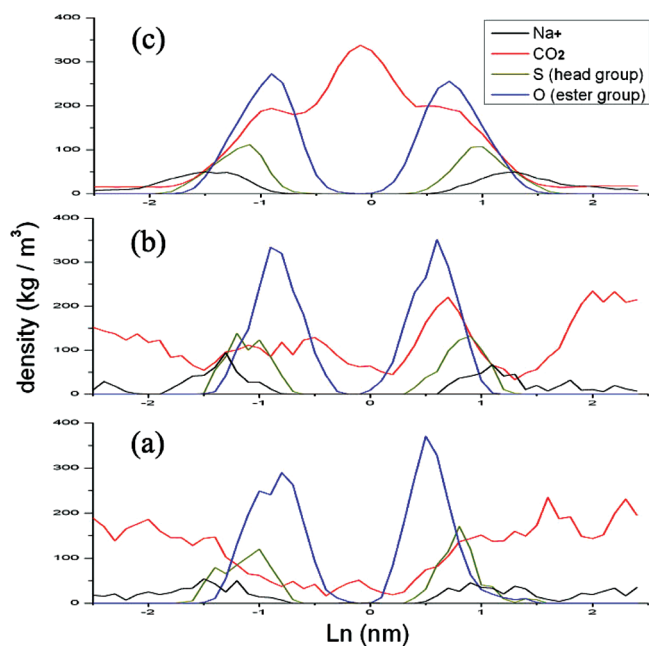


**Figure 5.** Density distributions of Na<sup>+</sup>, CO<sub>2</sub>, headgroup, and ester group along the normal direction of bilyaer averaged within (a) the first 20 ps, (b) 100 to 120 ps, and (c) 2000 to 3000 ps.

In eq 3,  $[CO_2]_{micelle}^c$  is the critical concentration of CO<sub>2</sub> in the micelle at the morphological transition, and  $p_{tran,CO_2}$  is the pressure of CO<sub>2</sub> at the morphological transition. Therefore, an increase of the distribution factor  $K^\ominus$  results in a reduction in transition pressure, which is more convenient to control the morphological transition. To this end, the hydrophobic tail of the surfactant must possess a favorable affinity for CO<sub>2</sub>, which contributes to the solubility of CO<sub>2</sub> in the micelle phase. Partially

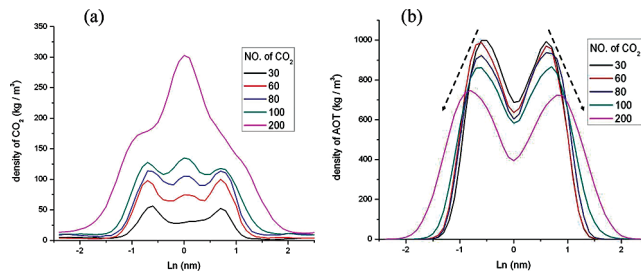


**Figure 6.** (a) Density distribution of CO<sub>2</sub> along the normal direction of bilayer in systems with 30, 60, 80, 100, and 200 CO<sub>2</sub> molecules, respectively. (b) Density distribution of AOT4 in systems with 30, 60, 80, 100, and 200 CO<sub>2</sub> molecules.

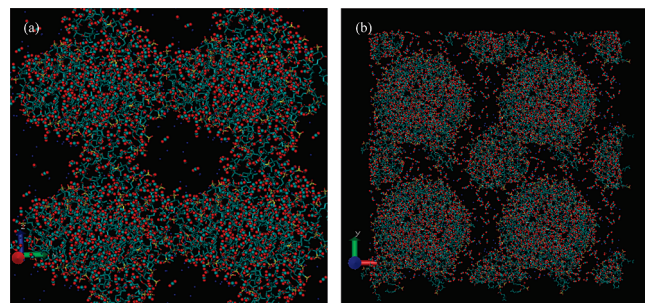


**Figure 7.** (a) 3D cubic network; (b) spherical micelle. Water is not shown for clarity. The snapshot shows a supercell of 2 × 2 × 2 simulation box. Display model and color code are the same as in Figure 1.

and fully fluorinated surfactants may be the best candidates because of their excellent solubility in supercritical CO<sub>2</sub>.<sup>35–37</sup> According to the “electron density matching” theory, surfactants with similar electron densities to CO<sub>2</sub> are expected to be highly CO<sub>2</sub>-philic. As reported by Tabor et al., the electron densities of CO<sub>2</sub>, AOT, and DiHCF<sub>4</sub> (sodium bis(1*H*,1*H*,5*H*-octafluoro-*n*-pentyl)sulfosuccinate) and DiCF<sub>4</sub> (sodium bis(1*H*,1*H*-perfluoro-*n*-pentyl)sulfosuccinate) are about 0.89, 0.4, 0.89, and 0.92 e/Å<sup>3</sup>, respectively.<sup>27</sup> Despite the same headgroup, AOT, DiHCF<sub>4</sub>, and DiCF<sub>4</sub> possess different tails as shown in Figure 8. DiHCF<sub>4</sub> and DiCF<sub>4</sub> exhibit high activity in the interface between water and supercritical CO<sub>2</sub>, while AOT turns out to be CO<sub>2</sub> inactive.<sup>38</sup> The chemical characteristic of the tail group is important to surfactant activity. A slight modification of tail group may lead to a substantial difference in surfactant property. It was reported by Wallen and Raveendran<sup>39</sup> that vinyl acetate chains are able to promote CO<sub>2</sub>-philicity. On this basis, Enick and Beckman et al. designed and synthesized a new AOT analogue AO-VAc, which bears vinyl acetate oligomeric chains.<sup>37</sup> Eastoe and Steytler<sup>27,38</sup> also developed a new AOT analogue AOK, which has a carbonyl group in each tail. Carbonyl groups exhibit strong Lewis acid and base interactions with CO<sub>2</sub>,<sup>40–42</sup> which contribute to the solubility of the surfactant in supercritical CO<sub>2</sub>.<sup>43</sup> On the basis of the importance of

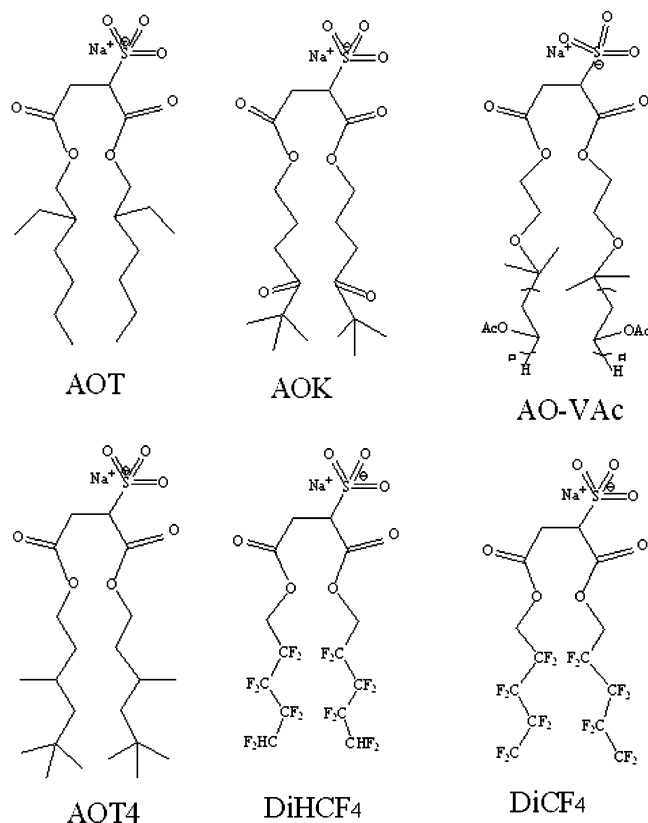


**Figure 8.** Surfactants AOT, AOT4, AOK, AO-VAc, DiHCF<sub>4</sub>, and DiCF<sub>4</sub>.

surfactant chain-tip chemical structure on liquid–liquid interfacial properties, the oxygenated surfactants AO-VAc and AOK show excellent CO<sub>2</sub> compatibility. Compared with CO<sub>2</sub>-inactive surfactant AOT, the lamellar bilayer formed by CO<sub>2</sub>-active surfactants mentioned above is expected to change into the spherical micelle at a lower transition pressure.

#### 4. Conclusions

The microstructure transition of surfactant in aqueous solution induced by CO<sub>2</sub> has been investigated by molecular dynamics simulations. Two strategies were adopted in our simulations. In the first, CO<sub>2</sub> molecules were added into the surfactant system with a preformed lamellar bilayer. In the second, surfactants were ranged homogeneously and CO<sub>2</sub> were added randomly. Both strategies yielded similar structures, consisting of lamellar bilayer. The thickness of bilayer and average area per surfactant are approximately 19.2 Å and 83.3 Å<sup>2</sup>. The density of AOT4 bilayer shows a bimodal distribution along the normal direction. The bilayer has a sandwich structure with a hydrophobic layer composed of hydrocarbon tails in the center and a hydrophilic layer formed by hydrated headgroups located on both sides. Na<sup>+</sup> counterions distribute around the headgroups due to the Coulombic interactions. The dissolved CO<sub>2</sub> is first adsorbed near the ester groups. With increasing amount of CO<sub>2</sub>, a condensed CO<sub>2</sub> layer occurs in the center of the lamellar bilayer. The bilayer becomes loose and unstable as swollen by CO<sub>2</sub> and expands with more CO<sub>2</sub> dissolved. Driven by surface tension, the lamellar bilayer tends to reduce its surface area; consequently, a microstructure transition finally occurs. A 3D cubic network was observed at the simulation box of 5 × 5 × 5 nm<sup>3</sup> due to the influence of neighboring images. Nevertheless, the spherical micelle was formed when a larger simulation box was adopted. CO<sub>2</sub>-active fluorinated surfactants (e.g., DiHCF<sub>4</sub> and

DiCF<sub>4</sub>) and oxygenated AOT analogues (e.g., AO-VAc and AOK) are proposed to substitute CO<sub>2</sub>-inactive AOT. They are expected to reduce the critical pressure in the microstructure transition.

The microscopic insight provided in this study is useful to unravel the mechanism of microstructure transition of surfactant induced by CO<sub>2</sub>, and thus monitor the microstructures. Precise control of the microstructures of surfactant by CO<sub>2</sub> shows attractive potential in the synthesis of nanomaterials. It is environmentally benign without using any organic solvent. It is also easy to postprocess compared with the conventional method because there is no need to remove additives such as cosurfactants and salts.

**Acknowledgment.** Financial support for this work was provided by the National Natural Science Foundation of China (Nos. 20776040, 20876041, 20736002), National Basic Research Program of China (2009CB219902), Program for Changjiang Scholars and Innovative Research Team in University of China (Grant IRT0721), the 111 Project of China (Grant B08021), and the National University of Singapore (R-279-000-238-112).

**Supporting Information Available:** Additional information as identified in the text. This material is available free of charge via the Internet at <http://pubs.acs.org>.

#### References and Notes

- Prieto, N. E.; Lilenthal, W.; Tortorici, P. L. *J. Am. Oil Chem. Soc.* **1996**, *73*, 9.
- Sánchez, M. C.; Berjano, M.; Guerrero, A.; Gallegos, C. *Langmuir* **2001**, *17*, 5410.
- Rosen, M. J.; Wang, H. Z.; Shen, P. P.; Zhu, Y. Y. *Langmuir* **2005**, *21*, 3749.
- Laurent, N.; Lafont, D.; Dumoulin, F.; Boullanger, P.; Mackenzie, G.; Kouwer, P. H. J.; Goodby, J. W. *J. Am. Chem. Soc.* **2003**, *125*, 15499.
- Brake, J. M.; Daschner, M. K.; Luk, Y.-Y.; Abbott, N. L. *Science* **2003**, *302*, 2094.
- Attard, G. S.; Glyde, J. C.; Goltner, C. G. *Nature* **1995**, *378*, 366.
- Attard, G. S.; Bartlett, P. N.; Coleman, N. R. B.; Elliott, J. M.; Owen, J. R.; Wang, J. H. *Science* **1997**, *278*, 838.
- Stupp, S. I.; Braun, P. V. *Science* **1997**, *277*, 1242.
- Tao, C.; Zheng, S. P.; Möhwald, H.; Li, J. B. *Langmuir* **2003**, *19*, 9039.
- Simmons, B. A.; Li, S. C.; John, V. T.; McPherson, G. L.; Bose, A.; Zhou, W. L.; He, J. B. *Nano Lett.* **2002**, *2*, 263.
- Ranjan, R.; Vaidya, S.; Thaplyal, P.; Qamar, M.; Ahmed, J.; Ganguli, A. K. *Langmuir* **2009**, *25*, 6469.
- Lelong, G.; Bhattacharyya, S.; Kline, S.; Cacciaguerra, T.; Gonzalez, M. A.; Saboungi, M.-L. *J. Phys. Chem. C* **2008**, *112*, 10674.
- Xia, Y. D.; Mokaya, R. *J. Phys. Chem. B* **2006**, *110*, 3889.
- Gradzielski, M. *Curr. Opin. Colloid Interface Sci.* **2003**, *8*, 337.
- Imai, M.; Nakaya, K.; Kato, T.; Takahashi, Y.; Kanaya, T. *J. Phys. Chem. Solids* **1999**, *60*, 1313.
- Escalante, J. I.; Gradzielski, M.; Hoffmann, H.; Mortensen, K. *Langmuir* **2000**, *16*, 8653.
- Richtering, W. *Curr. Opin. Colloid Interface Sci.* **2001**, *6*, 446.
- Dan, N.; Shimon, K.; Pata, V.; Danino, D. *Langmuir* **2006**, *22*, 9860.
- Nakamura, N.; Tagawa, T.; Kihara, K.; Tobita, I.; Kunieda, H. *Langmuir* **1997**, *13*, 2001.
- Macdonald, P. M.; Strashko, V. *Langmuir* **1998**, *14*, 4758.
- Wang, W.; Lu, W. S.; Jiang, L. *J. Phys. Chem. B* **2008**, *112*, 1409.
- Zhang, J. L.; Han, B. X.; Li, W.; Zhao, Y. J.; Hou, M. Q. *Angew. Chem., Int. Ed.* **2008**, *47*, 10119.
- Giner-Casares, J. J.; Camacho, L.; Martín-Romero, M. T.; Cascales, J. J. L. *Langmuir* **2008**, *24*, 1823.
- Dominguez, H. *J. Phys. Chem. B* **2007**, *111*, 4054.
- Gurtovenko, A. A.; Vattulainen, I. *J. Am. Chem. Soc.* **2007**, *129*, 5358.
- Sammalkorpi, M.; Karttunen, M.; Haataja, M. *J. Am. Chem. Soc.* **2008**, *130*, 17977.
- Tabor, R. F.; Gold, S.; Eastoe, J. *Langmuir* **2006**, *22*, 963.
- Oostenbrink, C.; Villa, A.; Mark, A. E.; Van Gunsteren, W. F. *J. Comput. Chem.* **2004**, *25*, 1656–1676.
- Becke, A. D. *J. Chem. Phys.* **1988**, *88*, 2547.

- (30) Lee, C.; Yang, W.; Parr, R. G. *Phys. Rev. B* **1988**, *37*, 785.
- (31) Hirshfeld, F. L. *Theor. Chim. Acta B* **1977**, *44*, 129.
- (32) Grillo, I.; Levitz, P.; Zemb, Th. *Langmuir* **2000**, *16*, 4830.
- (33) Nave, S.; Eastoe, J. *Langmuir* **2000**, *16*, 8733–8740.
- (34) Matheson, I. B. C.; King, A. D. *J. Colloid Interface Sci.* **1978**, *66*, 464.
- (35) Eastoe, J.; Gold, S. *Phys. Chem. Chem. Phys.* **2005**, *7*, 1352.
- (36) Harrison, K.; Goveas, J.; Johnston, K. P.; O'Rear, E. A. *Langmuir* **1994**, *10*, 3536.
- (37) Hoefling, T. A.; Enick, R. M.; Beckman, E. J. *J. Phys. Chem.* **1991**, *95*, 7127.
- (38) Eastoe, J.; Gold, S.; Steytler, D. C. *Langmuir* **2006**, *22*, 9832.
- (39) Raveendran, P.; Wallen, S. L. *J. Am. Chem. Soc.* **2002**, *124*, 7274.
- (40) Pitt, A. R.; Morley, S. D.; Burbidge, N. J.; Quickenden, E. L. *Colloids Surf., A* **1996**, *114*, 321.
- (41) Rindfleisch, F.; DiNoia, T. P.; McHugh, M. A. *J. Phys. Chem.* **1996**, *100*, 15581.
- (42) Meredith, J. C.; Johnston, K. P.; Seminario, J. M.; Kazarian, S. G. *J. Phys. Chem.* **1996**, *100*, 10837.
- (43) Kazarian, S. G.; Vincent, M. F.; Bright, F. V.; Liotta, C. L.; Eckert, C. A. *J. Am. Chem. Soc.* **1996**, *118*, 1729.

JP910253B